Sustainable Engineering Materials
ISSN: 3105-1960 (Print); ISSN: 3105-1979 (Online)
http://www.sustain-dpl.com/picnews.asp?id=177
DOI: 10.54113/j.suem.2026.000024

ORIGINAL ARTICLE

Experimental investigation on Mode I interlaminar fracture behavior of laminated flattened-bamboo composite measured by VIC-3D technique

Yue Chen[a, b], Yijia Guo[c], Haitao Li[a, b*], Jingru Zhang[a, b], Wei Xu[a, b], Xin Xue[a, b], Conggan Yuan[d], Priscilla Omouendze Mouaragadja[e], Shan Zhao[f], Rodolfo Lorenzo[g]

[a] Jiangsu Carbon Sequestration Materials and Structural Technology of Bamboo & Wood Research Center, Nanjing Forestry University, Nanjing 210037, China
[b] Joint International Research Laboratory for Bio composite Building Materials and Structures, Nanjing Forestry University, Nanjing 210037, China
[c] School of International Education, Tianjin Chengjian University, Tianjin 300384, China
[d] Jiangxi Feiyu Bamboo Materials Holding Co., LTD., Yichun 330700, China
[e] National College for Water and Forestry of Gabon, Libreville 3960, Gabon
[f] Nanjing Zidong Investment Development Group Co., Ltd., Nanjing 210000, China
[g] College of Civil Engineering, University College London, London WC1E 6BT, UK.
[*]Corresponding Author: Haitao Li, Professor, E-mail: lhaitao1982@126.com

Abstract: Mode I fracture tests, with loading perpendicular to the grain and crack propagation parallel to the grain, were performed on 10 groups of laminated flattened-bamboo composite (LFBC) specimens using the compact tension (CT) method, and crack extension was monitored by VIC-3D (video image correlate, 3D) technique. Nine of the groups were interlaminar (RL) fracture considering specimen thickness (*B*) and initial crack length to width ratio (*a*/*W*), and one group was standard specimens for intralaminar (TL) fracture as a control. It was shown that the failure mechanism of TL fracture was fiber fracture and ground tissue damage, while RL fracture was adhesive failure accompanied by a small amount of fiber fracture. The difference in the failure mechanism determined the uncertainty of crack extension in RL, while the crack extension in TL was continuous. On this basis, different forms of load-displacement curves and load-crack curves were analyzed. In addition, *a*/*W* had no effect on the fracture toughness of RL, while the condition value of fracture toughness gradually increased and reached stability with increasing thickness *B*. The RL fracture toughness of LFBC obtained from the test was 20.8 MPa·mm$^{1/2}$. The tensile strain field during crack extension was always concentrated at the crack tip, while the compressive strain appeared at the bottom of the specimen. An empirical equation for predicting the critical load of RL fracture was proposed by fitting to the test data.

Keywords: laminated flatted-bamboo composite, Mode I fracture, crack propagation, failure modes, fracture toughness

1 Introduction

Due to the excessive energy consumption of traditional building materials, low-carbon, eco-friendly and renewable new-type building material systems are becoming a hot topic in today's construction industry, one of the most representative materials is bio-based composite [1, 2]. With its short growth cycle, light weight, high toughness and good mechanical properties, bamboo has become

Received: 24 October 2025; Received in revised form: 4 August 2026; Accepted: 8 August 2026

a highly sought-after bio-building material [3]. However, raw bamboo is limited in size and shape, as well as its physical and mechanical properties vary along the radial direction, making it difficult to be widely used in practical engineering [4, 5]. These problems have been solved by the emergence of laminated bamboo lumber (LBL) [6, 7], which is a composite of equal-thickness bamboo strips obtained by shaving the excess from raw bamboo, allowing for a more homogeneous material, whose size and shape can also be designed and processed according to needs. Existing research has confirmed the excellent mechanical properties of LBL, which has been widely used in construction structures [8].

However, LBL still leaves the disadvantage of low material utilization. In this regard, a material optimized on the basis of LBL, laminated flattened-bamboo composite (LFBC), was developed by scholars [9]. LFBC is processed without shaving off the inner and outer layers of bamboo, and just by softening and flattening 1/2 or 1/4 of the bamboo tube, large-area bamboo panel units can be obtained for lamination [10]. At present, the technology of producing LFBC is already mature, which can increase the material utilization rate of LFBC by more than 20% compared with LBL, meanwhile, the production efficiency is greatly improved, also the labor cost is lowered [11]. Yang et al. [12] tested the basic mechanical properties of LFBC in three orthogonal directions and found that the measured performances were comparable to those of other structural biomaterials. Chen et al. [13] investigated the dowel-bearing properties of LFBC, and Zhang et al. [14] experimentally studied the bonded anchorage properties of LFBC joints with glued reinforcement. Nevertheless, studies on other mechanical behaviors of LFBC (e.g., fracture properties) are still in a lack and need to be supplemented by more experiments.

The special fiber structure of bamboo determines its high toughness, but low tensile strength in the perpendicular-to-grain direction, and prone to longitudinal cracking characteristics [15]. Especially, for engineered bamboo, it is difficult to avoid pores and micro-cracks in the manufacturing process. These initial defects are likely to cause cracks to propagate internal to the material during the use of its members, and fracture damage occurs before yielding, reducing the safety factor and service life of the structure [16, 17]. Crack propagation is divided into three modes [18,19]: Mode I, the opening crack; Mode II, the slippage crack; Mode III, the tearing crack. Among them, Mode I is the most likely to occur, and the other two modes are accompanied by the appearance of Mode I. Therefore, the Mode I fracture properties are the most fundamental and essential for exploring the fracture behavior of engineered bamboo as well as vital factors in the design of structures [20].

There have been some reports on Mode I fracture studies of moso bamboo and engineered bamboo. Using acoustic emission technique, Chen et al. [21] measured three kinds of fracture behaviors during bending in the inter-nodal part of moso bamboo: matrix damage, fiber separation and fiber fracture. An et al. [22] tested the bending fracture characteristics in different parts of moso bamboo respectively with the finding that the strength of the bamboo outer layer (fiber-dense layer) was much higher than that of the bamboo inner layer. Based on the different cell wall structures of fibers, Chen et al. [23] determined the main types of fracture: brittle fracture occurred in fibers with few layers; fracture transformed to ductile damage as the number of layers increased. Liu et al. [24] used scanning electron microscopy to observe the important fracture features of matrix cracking, interfacial separation, fiber bridging and splitting of cell wall layers in moso bamboo, confirming that rational weak interfaces are beneficial to improve the fracture toughness of bamboo. Most of the existing studies on engineered bamboo have focused on intralaminar fractures, which are similar to those of raw bamboo, but fewer studies have been conducted on interlaminar fractures. Liu et al. [25] investigated the Mode I interlaminar fracture behavior of laminated bamboo composites finding that no significant fiber bridging was observed during the test and the damage mode was mainly brittle fracture. Sheng [17] tested the interlaminar fracture properties of bamboo integrates concluding that interlaminar fracture did not have a non-negligible plastic extension zone and exhibited significant brittleness compared to intralaminar fracture. In fact, interlaminar fracture, which is influenced by the common action of the adhesive and the bamboo material, also tends to have lower fracture toughness and is a more dangerous mode than intralaminar fracture.

In summary, Mode I fracture characteristics are essential for assessing the mechanical properties of engineered bamboo materials, and there is a lack of research on this aspect of LFBC. In this paper, based on the fracture failure modes, the interlaminar Mode I fracture properties of LFBC under different influencing factors were tested and compared with those of intralaminar fracture in order to investigate the influence of failure modes on intralaminar and interlaminar fracture. The aim is to supplement the mechanical properties of this material and to provide reference for the development of relevant testing standards and engineering design.

2 Test design

2.1 Materials

The raw material was 3-4 years old moso bamboo from Jiangxi Province, China, which was processed into LFBC and manufactured into test specimens by Jiangxi Feiyu Bamboo Materials Holding Co., LTD. As shown in **Fig. 1**, the difference between LFBC and LBL is that the basic unit of LBL is the bamboo strip in the middle of the arc-shaped bamboo sheet (the strip width is usually only 21 mm), while the basic unit of LFBC is the flat plate obtained by flattening the arc-shaped bamboo sheet (the plate width can reach 100 mm). The processing steps of LFBC were as follows: Using urea-formaldehyde resin as the adhesive, these flat plates were glued into veneers at 95°C, under a vertical pressure of 12 MPa and a horizontal pressure of 4 MPa. These veneers were then brushed with adhesive, stacked, and pressed under 18 MPa of positive pressure for two hours to produce LFBC. The basic mechanical properties of this material were tested as per ASTM D143-2014 [26] standard and the average values of the test results are shown in **Table 1** [13] (each trial was repeated 20 times).

Table 1. The mechanical properties of LFBC [13]

	Compression			Tension			Density/kg/m^3	Moisture content
	R	T	L	R	T	L		
strength/MPa	43.1	19.0	56.2	1.8	4.3	106.9	743	8.5%

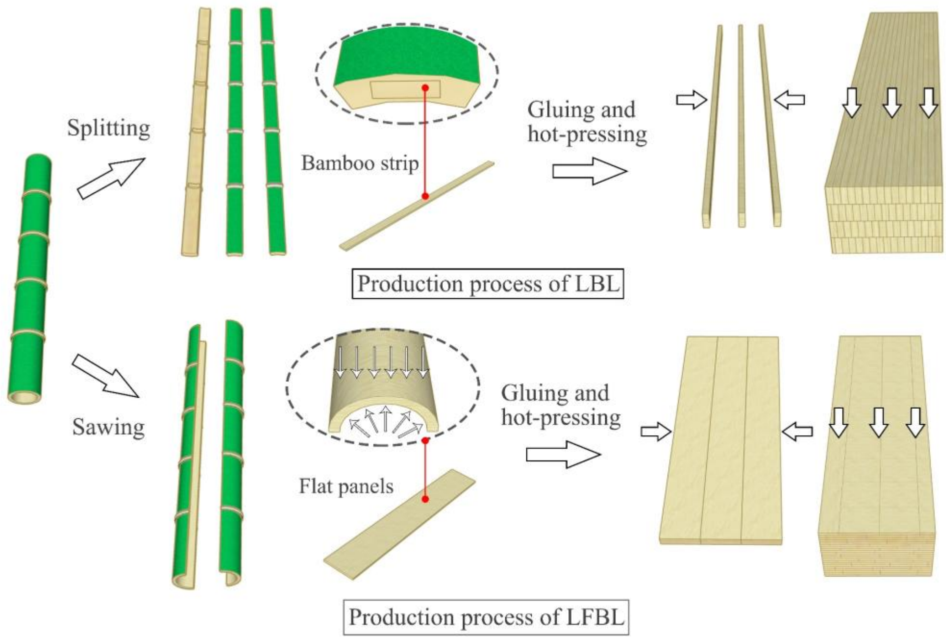

Fig. 1. The manufacturing process of LBL and LFBC

2.2 Specimen design and test methed

2.2.1 Design of groups and loading scheme

Fig. 2 showed the diagrams and photos of the specimens, where "L" indicated the direction of fiber growth, "R" indicated the direction perpendicular to the bamboo plates, and "T" meant that the bamboo plates were flattened along this direction; the first letter in the naming of the specimen type (TL/RL) referred to the loading direction, and the second letter referred to the crack extension direction. As per ASTM E399 [27], 10 groups of LFBC compact tension (CT) specimens were tested for Mode I fracture characteristics, with 6 repetitions of each group. Nine of the groups were interlaminar fracture tests (the test specimens were of RL type) with thickness (B) and prefabricated crack length (a_0) as variables; the cracks of these specimens were prefabricated on the gluing surface between two layers of bamboo veneers; the gradient of B was set as follows: 15 mm, 20 mm, 25 mm, 30 mm, 35 mm, and the a0 was varied as follows: 20 mm, 22.5 mm, 25 mm, 27.5 mm, 29 mm; the specimen group with B of 25 mm and a_0 of 25 mm was set as the standard group. In addition, a group for intralaminar fracture tests (the test specimens were of TL type) with B=25 mm and a_0=25 mm was set up as a control. The detailed naming and grouping of the specimens were shown in **Table 2.** The crack width of all specimens was 2 mm, and a fine gap of about 1 mm in length was manually cut at the crack tip to guide the crack extension.

The capacity of the universal testing machine used for loading was 50 kN, and the loading ratio was set to 0.5 mm/min. The U-shape fixture used for tension was made of steel with a carbon content of 0.45%. Pre-loading was carried out before the test, and the load values and test phenomena were recorded during the test, while the displacement data were captured by the VIC-3D system. The test equipment and site were provided by the structural laboratory of Nanjing Forestry University.

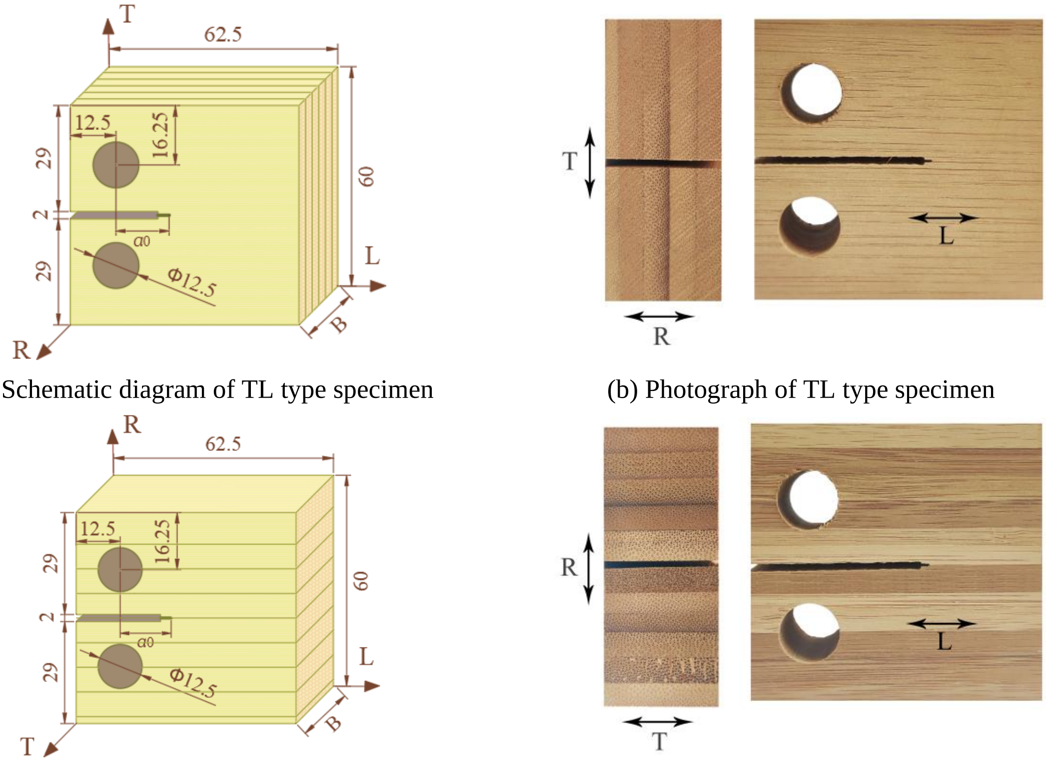

(a) Schematic diagram of TL type specimen (b) Photograph of TL type specimen

(c) Schematic diagram of RL type specimen (d) Photograph of RL type specimen

Fig. 2. Specimen type and dimensions (Unit: mm)

2.2.2 Determination of critical stress intensity factor and critical load

When the stress near the crack tip is in a plane strain state and the plastic deformation here is restrained, the resistance of the material to crack extension is called the stress intensity factor (K_{IC}). Often K_{IC} is also used to characterize the fracture toughness of a material, that is, the material fracture is considered to occur when the stress intensity factor reaches K_{IC}. In this study, Eq. (1) specified by ASTM E399 standard was used to calculate the conditional value (K_Q) of K_{IC}.

$$K_Q = (P_Q / BW^{1/2}) \times f(a/W) \tag{1}$$

Where the parameters represented, respectively, P_Q: critical load, B: thickness of the specimen; W: effective width of the specimen (50 mm for this study); a: length of the initial crack; $f(a/W)$: the geometric coefficient for CT specimens, calculated according to Eq. (2). If the test was effective (i.e., K_{IC}=K_Q), two conditions needed to be satisfied: 1) B and a were both over $2.5(K_Q/\sigma_s)^2$, where σ_s was 0.2% tensile yield strength; 2) (P_{max}/P_Q) <1.1, where P_{max} was the ultimate load. If it was not satisfied, thicker specimens should be replaced for testing.

$$f(x) = (2+x) \times \frac{0.886 + 4.64(x) - 13.32(x)^2 + 14.72(x)^3 - 5.6(x)^4}{(1-x)^{1.5}} \tag{2}$$

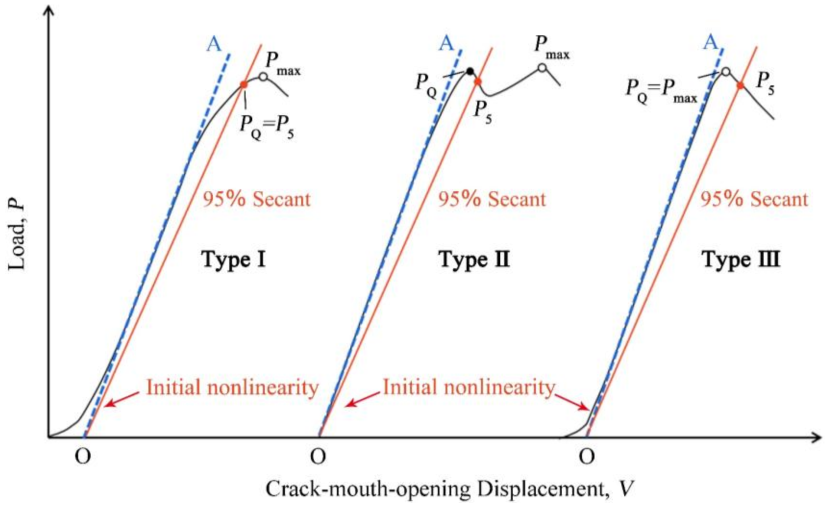

Fig. 3. Critical load positioning

As shown in **Fig. 3**, the method of locating P_Q: taking the intersection of line *OA* and *X*-axis as the origin *O*, where *OA* was the tangent line of the linear segment in the load-crack opening displacement (*P*-*V*) curve, a cut line OP_5 was drawn from the point *O* with a slope of 0.95 times the *OA* slope. If the load at P_5 exceeded the load at all preceding points (type I curve), then $P_Q = P_5$; if there existed a maximum load in front that was larger than P_5 (type II or III curve), then such maximum load was chosen as P_Q.

2.2.3 Observation of strain field and crack extension

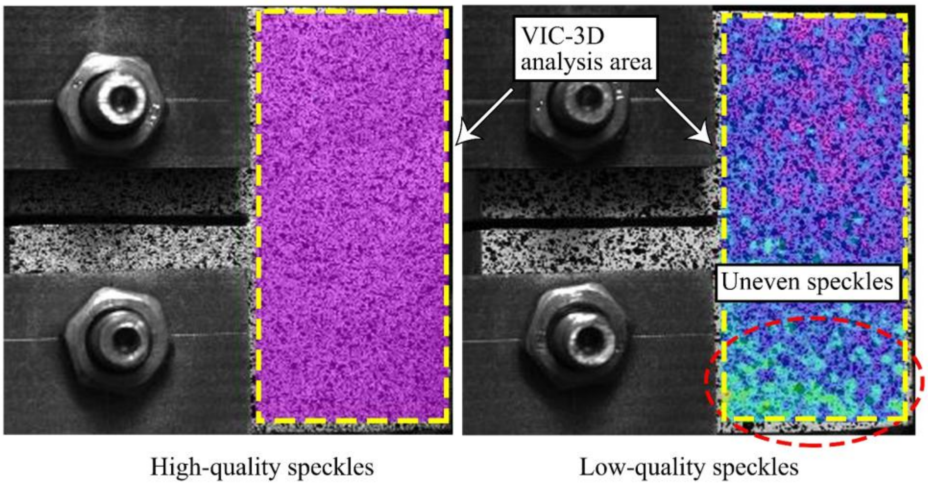

Fig. 4. Comparison of scattered spot quality

Since crack measurements are sub millimeter, the accuracy of the measuring equipment is very demanding. The core technology of VIC-3D system is the digital image correlation (DIC) principle, which is to measure the full-field 3D shape, displacement and strain at any point by tracking the change of surface speckles (pixel subsets) during object deformation with high-speed cameras, achieving displacement accuracy of 0.01 pixels and strain accuracy of 20~50 microstrain. The system includes the necessary equipment: two industrial cameras (Model No. GRAS-50S5M-C in spot gray) and a cold light source; software: Vic-sanp for acquisition control and Vic-3D for analysis; in addition to other auxiliary equipment, such as data transmission lines, calibration plates, levels and tripods. Before the test, speckles needed to be fabricated on the observation surface of the specimen: white matte paint was used to cover the original grain of the specimen, and then black matte paint was sprayed evenly to form spots of 3-5 pixels in size, while ensuring that the ratio of black to white in the view was about 1:1. The quality of the speckles has an influence on the measurement results. **Fig. 4** showed the imaging of different-quality speckles under VIC-3D system, and the high-quality speckles should ensure the uniform image color under static. During the test, VIC-3D system captured speckle images at 5Hz and matched each photo to the load value at the time of shot to analyze results.

3 Analysis of test results

The test results were shown in **Table 2**, where *P* and *K* were average values. A1~RS~A4 groups studied the factor for the ratio of crack length to specimen width (a/W); B1~RS~B4 groups researched the effect of specimen thickness; TS and RS groups studied the difference between Interlaminar and Intralaminar fracture. Too small specimen thickness would lead to test ineffective and affect the results (the method to judge whether the test is effective or not was shown in 2.2.2). Some studies give the minimum specimen thickness for fracture test of other engineered bamboo materials, but there is no reference on LFBC. In this study, some of the specimens in groups B1 and B2 were found to be ineffective (effective number < 6), and it was considered that the specimen thickness should be larger to ensure the effectiveness of the test.

Table 2. Specimen configurations and fracture test results

Type	Groups	a (mm)	a/W	B (mm)	P_Q (N)	P_{max} (N)	K_Q (MPa·mm$^{1/2}$)	Effective number
TL	TS	25	0.5	25	462.1 (6.9)	482.7 (6.3)	25.2 (6.9)	6
RL	RS	25	0.5	25	375.6 (5.5)	389.1 (5.7)	20.5 (5.5)	6
	A1	20	0.4	25	493.2 (5.1)	506.0 (5.2)	20.3 (5.1)	6
	A2	22.5	0.45		429.7 (4.0)	441.9 (4.4)	20.3 (4.0)	6
	A3	27.5	0.55		316.9 (3.7)	329.8 (2.6)	20.4 (3.7)	6
	A4	30	0.6		264.7 (8.7)	278.1 (8.0)	20.4 (8.7)	6
	B1	25	0.5	15	196.4 (10.5)	215.8 (11.0)	17.9 (10.5)	4
	B2			20	276.9 (12.8)	295.9 (12.7)	18.9 (12.8)	5
	B3			30	479.4 (7.8)	486.1 (7.0)	21.8 (7.8)	6
	B4			35	563.5 (3.3)	568.8 (2.9)	22.0 (3.3)	6

Note: Values in parentheses are CoVs (%)

3.1 Failure modes

Due to the small size of the CT specimen, its fracture process zone (FPZ) was short, and it was difficult to observe the distinct fiber bridging phenomenon. From the tip of the prefabricated crack to the specimen bottom, only one main crack extended horizontally, so that the specimen was divided into two complete halves, without apparent subsidiary cracks observed. However, there were differences in the fracture cross-sectional morphology presented by TL and RL specimens, and the brittleness degrees of specimen breaks were also different.

3.1.1 Failure mode of intralaminar (TL) fracture

Bamboo is an anisotropic material which has low longitudinal (along the fiber growth direction) interfacial strength but high transversal toughness, and the cracks are prone to propagate along the fibers or the ground tissue. As shown in **Fig. 5(a)**, although no distinct fiber bridging was found in the CT specimen during the test, the TL type of intralaminar fracture revealed that the specimen had a more tortuous crack, the fracture surfaces were rough, and there were fiber protrusions and pullouts. **Fig. 5(b)** was the photograph of the fracture surface under scanning electron microscopy (magnified 200x and 800x, respectively), which showed that in FPZ, some fibers were integral and smooth, with fragments of ground tissue (consisting of parenchyma cells) remaining on the surface, and some the fibers were pulled off and exposed. It indicated that the intralaminar fracture of bamboo was essentially the destruction of fibers and ground tissues. Thus, the fiber and parenchyma cells in the TL specimen effectively inhibited the crack extension, allowing the crack propagation during the test to be slow and continuous and to exhibit ductile damage.

(a) Macroscopic failure mode

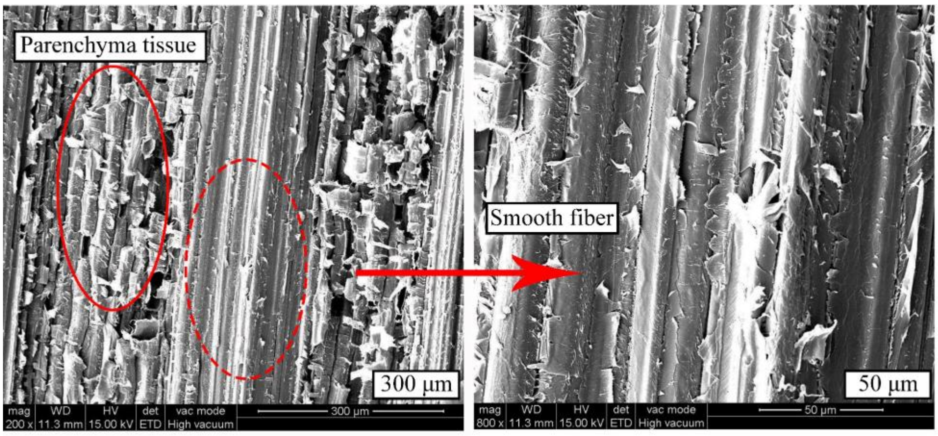

(b) Microscopic failure mode

Fig. 5. Failure mode of intralaminar (TL) fracture

3.1.2 Failure mode of interlaminar (RL) fracture

Compared with TL type, the process of interlaminar fracture of RL type was very fast and discontinuous. After reaching the critical load, the crack length would increase by a few millimeters in an instant and then remained for a while, and after continuing the loading for a period of time, the crack would extend rapidly again. This pattern was repeated until the specimen was completely split in half. The entire testing process for the RL specimen took less than half the time of the TL specimen.

As shown in **Fig. 6(a)**, the crack of RL specimen was very straight, and fracture surfaces were flat on which the residual adhesive patches were clearly visible, with no prominent fiber bundles. It was also evident in the micrograph (**Fig. 6(b)**) that the adhesive covered most area of the fracture surface, while a few fibers would be attached by the adhesive, causing them to be pulled off during the separation between the two parts of the specimen. Therefore, the interlaminar fracture of LFBC was essentially the failure of adhesive accompanied by a small amount of fiber fracture, and this damage mechanism determined the faster crack propagation with the specimen exhibiting pronounced brittleness.

(a) Macroscopic failure mode

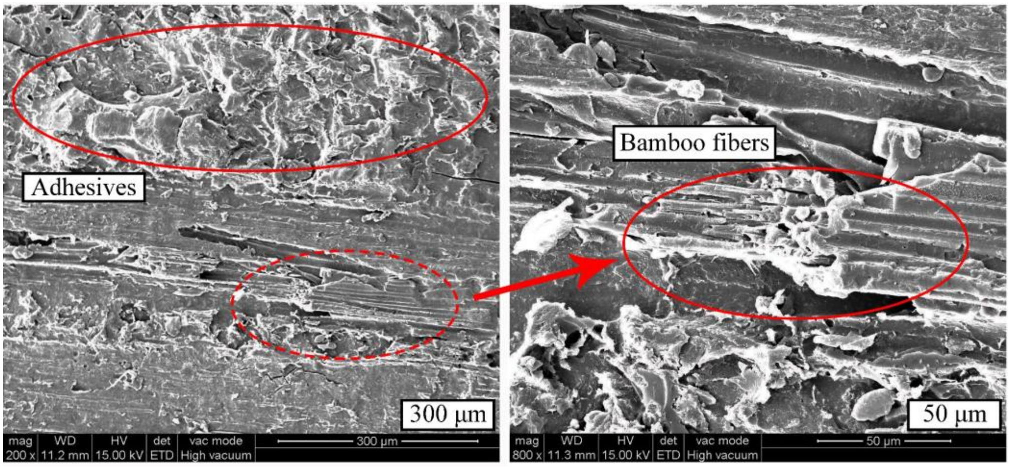

(b) Microscopic failure mode

Fig. 6. Failure mode of interlaminar (RL) fracture

3.2 Load-crack opening displacement (*P*-*V*) curves

Fig. 7 provided the *P*-*V* curves of each group. The curves in TS group were smooth and regular (all were type I curve in **Fig. 3**): at the early stage of loading, the surface material of the specimen contacting with the U-shaped fixture was gradually squeezed to dense, and the displacement grew fast; when the load increased to about 100 N, the elastic phase began and the curve grew linearly; as the load continuously growing, the curve slope declined progressively and the plastic deformation of the specimen occurred until the load reached P_{max}; after then, the crack propagation stabilized and the specimen bearing capacity decreased dramatically with the crack growth, this phase was the most time-consuming phase in the test process.

Before the elastic stage, the *P*-*V* curves of RL type specimens developed in the similar process as those of TL type specimens, while when entering the plastic deformation stage, the *P*-*V* curves of RL specimens began to vary randomly in a chaotic manner with no obvious pattern. Most of the curves dropped steeply after reaching the ultimate load (type III curve), showing apparent brittle characteristics, while a small portion of the curves would exhibit a fluctuating segment in which the P_Q value was obtained (type II curve).

The reasons for these differences were described in Section 3.1: in TL intralaminar fracture, the crack propagates along the fibers or ground tissue, which was a gradual and slow process, while in RL interlaminar fracture, it was the failure of the adhesive between the bamboo panels that caused the laminations to separate. Therefore, for RL specimens, the uneven brushing of glue, the presence of original pores and microcracks during processing could affect the fracture progression, and these factors increased the uncertainty in the development of the *P*-*V* curves.

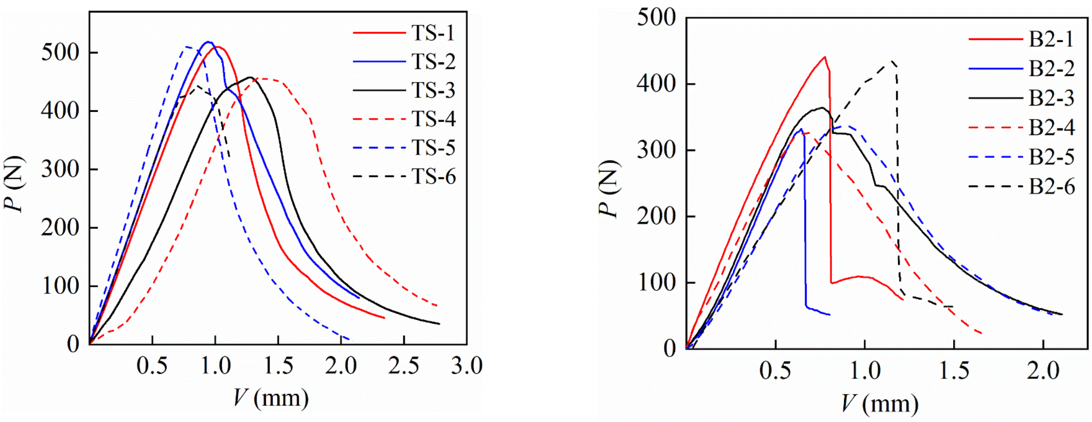

(a) Group TS

(b) Group RS

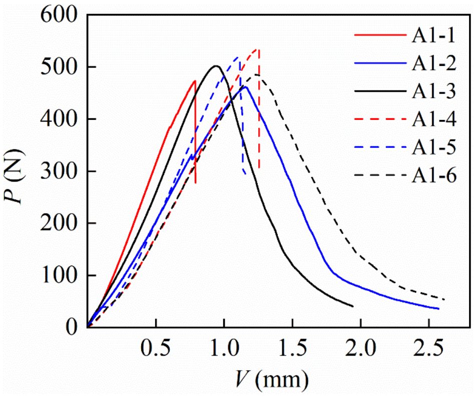

(c) Group A1

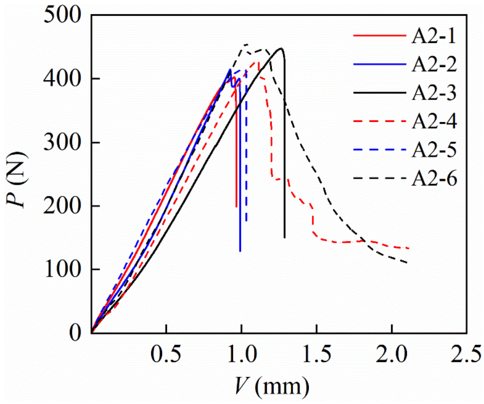

(d) Group A2

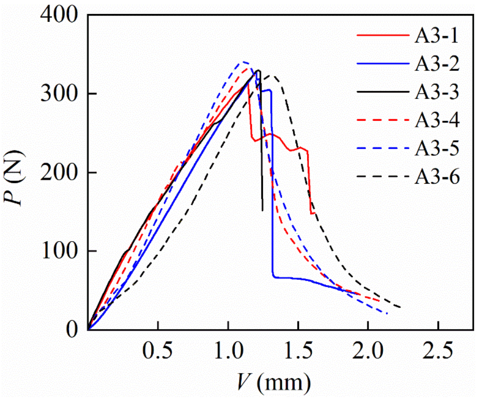

(e) Group A3

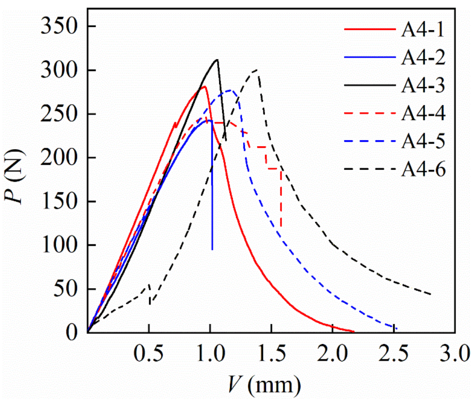

(f) Group A4

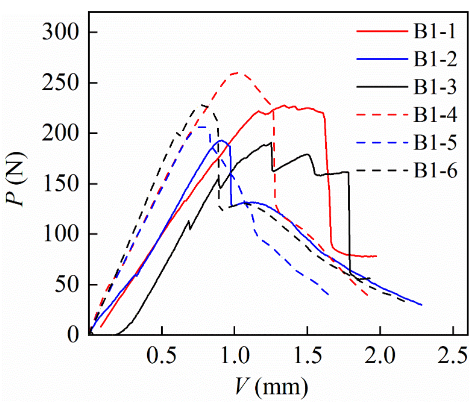

(g) Group B1

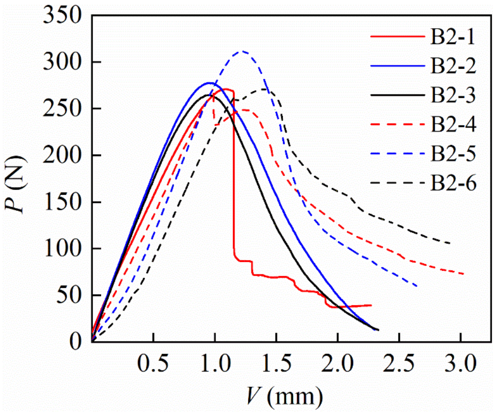

(h) Group B2

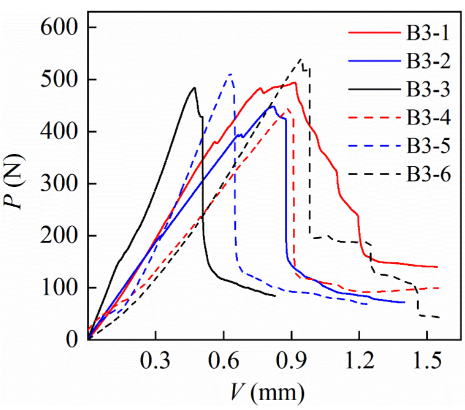

(i) Group B3

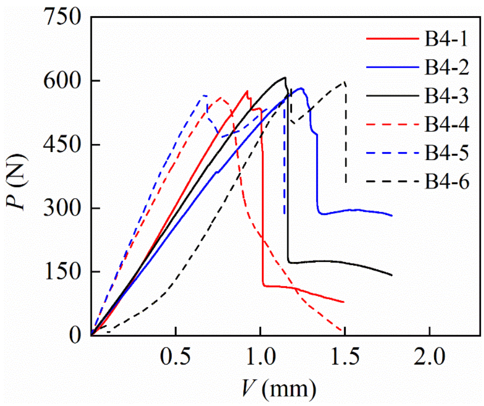

(j) Group B4

Fig. 7. *P*-*V* curves

3.3 Effect of dimensions on the fracture parameters of RL type

This section discussed the effect of *a/W* value and *B* on fracture parameters in RL specimens, including: the variation of *P* and K_Q between different groups and the trend of load-crack (*P*-*a*) curves.

3.3.1 Dimension effect on load and K_Q value

(1) Effect on load

Shown in **Fig. 8(a)**, with the increase of *a/W* from 0.4 to 0.6, the means of P_Q and P_{max} decreased almost linearly from 493.2 N to 264.7 N and from 506 N to 278.1 N, respectively, and the differences of P_Q and P_{max} were similar for each group. When the specimen thickness *B* was increased from 15 mm to 35 mm (**Fig. 8(b)**), the means of P_Q increased from 196.4 N to 563.5 N, and the means of P_{max} increased from 215.8 N to 568.8 N, with the values of P_Q and P_{max} getting increasingly close to each other. At the thickness of 35 mm, the P_Q was almost equal to P_{max}, which indicated that at this thickness, the specimen load capacity decreased sharply once the cracks initiated to extend.

(2) Effect on K_Q value

As depicted in **Fig. 8(c)**, there was almost no change in the K_Q value as the *a/W* value increased, indicating that the fracture of LFBC in the RL direction was not affected by the *a/W* value. However, **Fig. 8(d)** demonstrated that the fracture toughness condition value K_Q grew with increasing specimen thickness *B*. This growth trend was no longer apparent when the thickness reached 30 mm, since group B4 increased by 23% compared to group B1, while it only increased by 0.9% compared to group B3, proving that the fracture toughness reached stability at this time. Due to the existence of ineffective tests in both groups B1 and B2 (see **Table 2**), this study recommended that for the CT tests of LFBC in the RL direction, the specimen thickness should be at least that of the RS group, i.e., $B \geq 25$ mm. In this paper, the average of the K_Q values of groups A1~A4, RS and B3~B4, which satisfied the conditions, was taken as the Mode I fracture toughness of LFBC in the RL direction, with the value of K_{IC} = 20.8 MPa·mm$^{1/2}$.

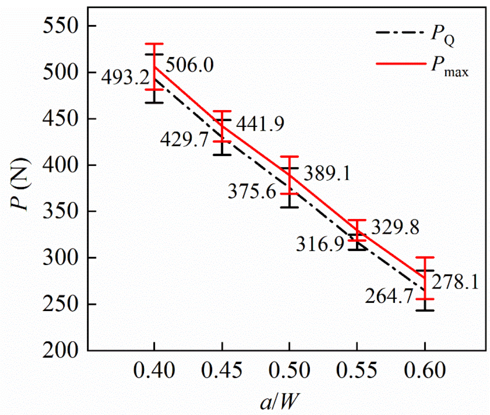

(a) Effect of *a/W* value on load

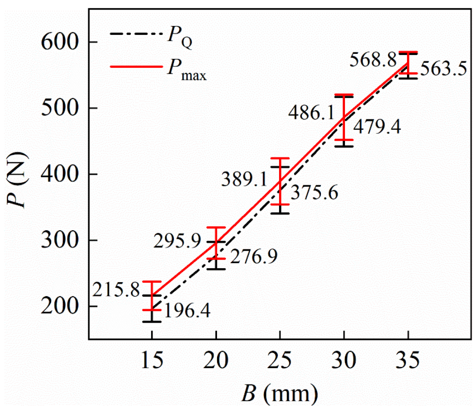

(b) Effect of *B* on load

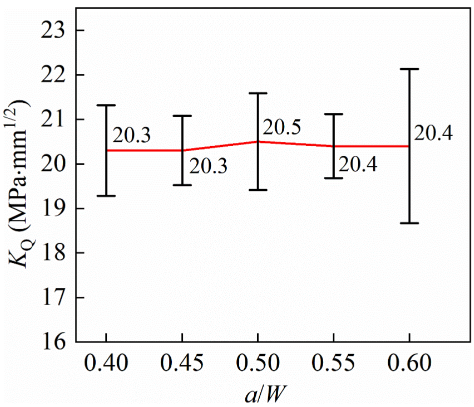

(c) Effect of *a/W* value on K_Q value

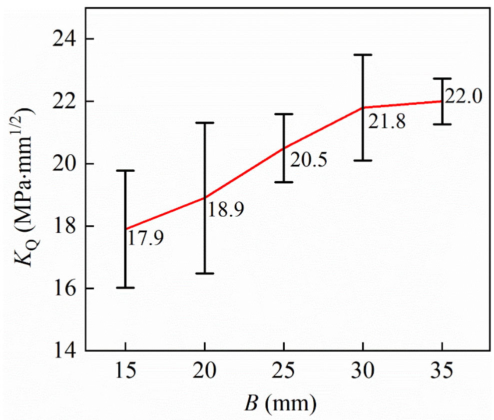

(d) Effect of *B* value on K_Q value

Fig. 8. Dimension effect on load and K_Q value

3.3.2 Dimension effect on load-crack (*P*-*a*) curves

During the test, VIC-3D system tracked the crack tip position throughout and obtained the crack length at each moment by calculating the total value of the newly generated crack length and the initial crack length, which was then matched with the corresponding load to derive the *P*-*a* curve.

Some fiber composites (e.g. glass fiber reinforced plastics [28, 29]), have been proved to possess self-consistency in crack propagation during fracture, i.e., when the components are of the same size, they will be in the same state as the cracks propagate to the equivalent length, regardless of how long the initial cracks are. It can be seen in **Fig. 9(a)** that the specimens of RL type followed the above trend in the initial stage of crack extension. However, as the crack length increased, the *P*-*a* curves for different initial crack lengths gradually diverged without regularity. The failure mechanism of RL interlaminar fracture led to the uncertainty in the late stage of crack development, i.e., the crack propagation rate, bearing load and cracking location all possessed randomness. As shown in **Fig. 9(b)**, the thicker the specimen, the faster the drop rate of the *P*-*a* curve, suggesting that the larger the B the rapider the loss of bearing capacity of the specimen during the crack development process.

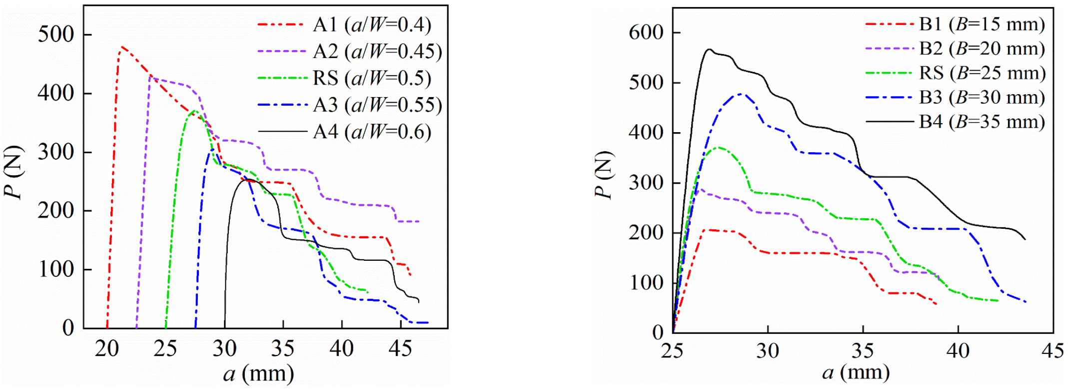

(a) Effect of *a*/*W* value on *P*-*a* curves (b) Effect of *B* value on *P*-*a* curves

Fig. 9. Dimension effect on *P*-*a* curves

3.4 Effect of loading direction on fracture parameters

This section discussed the effect of different loading (fracture) directions on the fracture parameters, i.e., the difference between the specimens of RS and TS groups in terms of load, fracture toughness, and *P*-*a* curves.

3.4.1 Effect on load and K_Q value

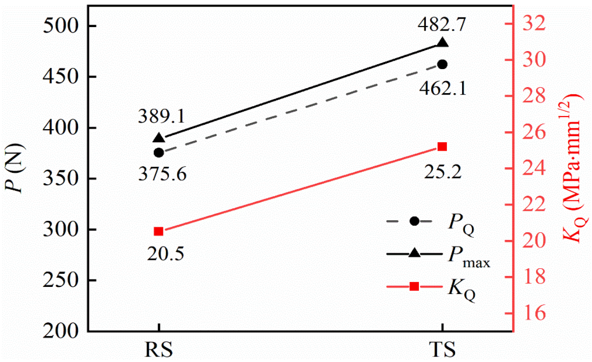

Fig. 10. Load and K_Q values for RL and TL types

As depicted in **Fig. 10**, the average ultimate load of the TS group was 482.7 N, which exceeded the 389.1 N of the RS group by about 24%; the average critical load of the TS group was 462.1 N which increased by about 23% compared with the 375.6 N of the RS group, and similarly the K_Q value of the TS group was also larger than that of the RS group. This showed that the specimens in the RL direction were weaker than those in the TL direction, both in terms of fracture performance and load carrying capacity. The reason for this was that the adhesion between the fibers was stronger, and the adhesive layers were often the weak part of the material. For laminated composites, how to prevent the adhesive from cracking is a constant topic in practical engineering applications.

3.4.2 Effect on *P*-*a* curves

The crack development in the RL direction was random and indeterminate as already explained in the previous section. The bond of the interlaminar adhesive would fail simultaneously over a certain area, causing crack extension to occur instantaneously and stabilize for some time before this extension occurs again when the adhesive failed in the next area. Therefore, the *P*-*a* curves of the RL type specimens were segmented wavy lines (**Fig. 11(a)**). However, the failure mode of TL-type specimens determined the continuity of crack extension, and thus the *P*-*a* curves of the TS group were smoother (**Fig. 11(b)**). In addition, the curves of the TS group were more concentrated and consistent in crack extension, while the curves of the RS group were more discrete.

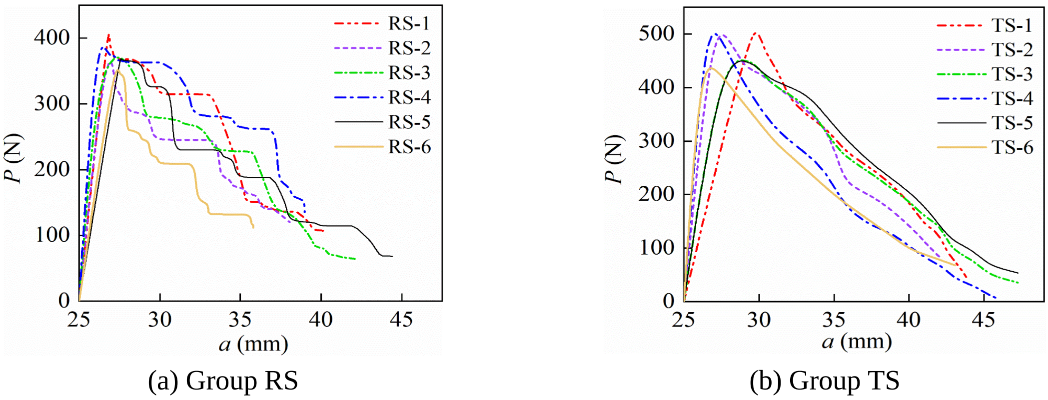

Fig. 11. *P*-*a* curves of specimens in TS and RS groups

3.5 Evolution of strain

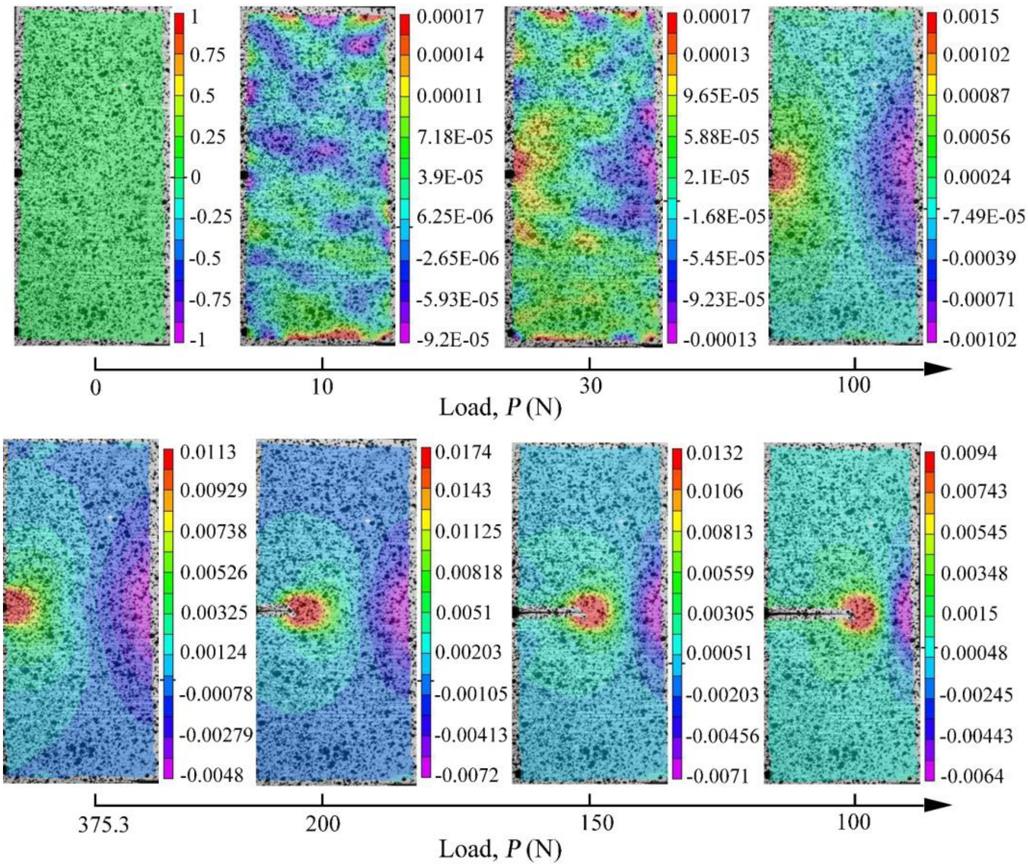

Fig. 12. Evolution of strain in a typical RL specimen

Before starting the acquisition, the calibration plate with small holes was moved and imaged on the surface of the specimen; the VIC-3D system could establish a three-dimensional coordinate system by comparing the actual distance between the small holes with the distance in the imaging; the triangulation system with two lenses effectively eliminated the optical distortion and rigid rotation of the object, thus measuring the deformation of the object accurately.

Fig. 12 illustrated the strain evolution of a typical RL specimen (P_Q = 375.3 N), including the phase of load growth before crack extension, and the phase of load decrease after crack extension started. In the case of unloading, there was no deformation on the surface of the specimen and just one color existed in the strain cloud. When the load was increased to about 10 N, the specimen surface began to deform slightly, but there was no obvious regularity, and multiple color blocks appeared in the cloud diagram. When the load increased to about 30 N, the strain value near the tip of the prefabricated crack was greater than 0, indicating that tensile strain was applied here, while compressive strain (strain value less than 0) was generated at the bottom of the specimen due to extrusion. With the further growth of the load, the tensile strain field was gradually concentrated towards the prefabricated crack tip, and an obvious red color patch could already be seen near the crack tip at 100 N. Once the strain at the crack tip reached the limit (the load reached P_Q), the crack started to extend, and the strain field was then transferred to the newly emerged crack tip. This process would continue until the crack extended to the specimen bottom with the maximum tensile strain reaching 0.0174.

3.6 Empirical equation

Empirical equations established on test data are often of great reference significance for predicting the value of a parameter of a material or member and play an active role in engineering design. The trend of crack extension of LFBC in the RL direction was shown to be uncertain in this study, but the critical load P_Q at the start of crack extension was predictable. Therefore, as depicted in **Fig. 13**, the two factors B and a/W were considered comprehensively, and the remaining experimental data after excluding groups B1 and B2 were fitted with a quadratic polynomial to obtain the P_Q equation shown in Eq. (3), with R^2 = 0.99, which showed a high degree of agreement. The predicted values of P_Q were substituted into Eq. (1) to derive the prediction values of K_Q. **Table 3** compared the K_Q values calculated using the prediction equation with the actual tested K_Q values, from which it could be seen that the maximum error was only 3.8%, proving the high accuracy of the equation.

$$P_Q = -0.103(BW/a)^2 + 21.897(BW/a) - 466.237 \tag{3}$$

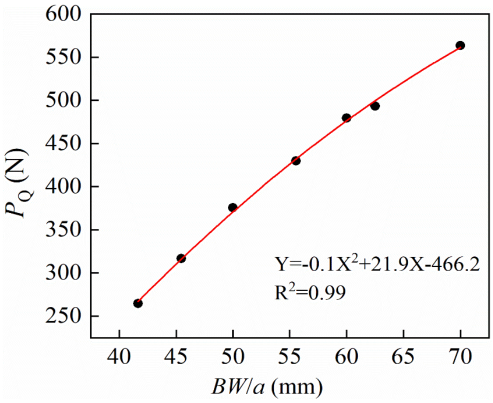

Fig. 13. Fitting curve of P_Q

Table 3. Calculated and tested values of K_Q

Groups	Calculated P_Q (N)	Calculated K_Q (MPa·mm$^{1/2}$)	Tested K_Q (MPa·mm$^{1/2}$)	Error
RS	378.8	20.7	20.5	0.9%
A1	511.9	21.1	20.3	3.8%
A2	441.8	20.8	20.3	2.8%
A3	322.6	20.7	20.4	1.8%
A4	272.7	21.1	20.4	3.0%
B3	487.8	22.2	21.8	1.8%
B4	576.8	22.5	22.0	2.4%

4 Discussion

(1) The failure modes of Mode I intralaminar (TL) fracture and interlaminar (RL) fracture of LFBC were observed by scanning electron microscopy. TL fracture was actually the destruction of fibers and ground tissues, which effectively inhibited the crack propagation so that the crack development in the test was slow and continuous and exhibited ductile damage. Accordingly, its *P-V* curves were smooth and regular, as well as the *P-a* curves were more centralized. The essence of RL fracture was adhesive failure accompanied by a small amount of fiber fracture, which led to its faster crack extension and the specimens exhibited obvious brittleness. After the crack started to extend, the rate and location of extension were uncertain, so the *P-V* curves and *P-a* curves of RL groups were observed to have more random and discrete morphology in the late stage of crack development. Also, the K_Q values of TL were higher than those of RL for the same dimensions. Improvement of the fabrication process can be considered in future studies to eliminate this variability, e.g., the adhesive can be replaced with phenolic resin, and the hot-pressing conditions can be changed. More research is needed to explore the effects of different fabrication processes on the fracture behavior of LFBC. In addition, tension in the RL direction should be avoided as much as possible in the engineering design, or carbon fiber reinforcement can be used.

(2) The effects of initial crack-to-width ratio (a/W) and specimen thickness (B) on the fracture properties of RL type were investigated. a/W had no effect on the fracture toughness, while the larger the B the more pronounced the brittle damage of the specimen, and too small B would lead to ineffective testing, so it is recommended that the specimen thickness should meet $B \geqslant 25$ mm for future CT tests of RL fracture. The fracture toughness of LFBC in the RL direction tested in this paper was $K_{IC} = 20.8$ MPa • mm$^{1/2}$. The crack extension of RL fracture was not self-similar, and the *P-a* curves diverged at the late stage of crack development.

(3) The strain evolution of a typical specimen of RL type was observed using the VIC-3D system. Compressive strains appeared at the bottom of the specimen and tensile strain fields were concentrated at the crack tip and moved with the crack extension, with a maximum strain value of 0.0174.

(4) In the RL direction, the critical load P_Q at the time when the crack first started to expand was predictable. In this paper, an empirical equation based on a/W and B was proposed to predict the P_Q value of the specimen. The predicted P_Q value was used to calculate K_Q, and the maximum error was only 3.8%, indicating that the empirical equation was highly accurate.

Acknowledgement

The writers gratefully acknowledge Nianqiang Zhou, Longlong Zhao, Chen Chen, Bingyu Jan, Tingting Ling, Dong Yang, Wenjing Zhou and others from the Nanjing Forestry University for helping with the tests.

Funding Statement

This work was supported by the National Natural Science Foundation of China (No. 51878354 & 51308301); the Natural Science Foundation of Jiangsu Province (No. BK20181402 & BK20130978). Any research results expressed in this paper are those of the writer(s) and do not necessarily reflect the views of the foundations.

CRediT authorship contribution statement

Yue Chen: Investigation, Formal analysis, Writing - original draft. **Yijia Guo:** Investigation, Formal analysis, Writing - original draft. **Haitao Li:** Conceptualization, Funding acquisition, Supervision, Investigation, Formal analysis, Writing - original draft. **Jingru Zhang:** Investigation, Writing - review & editing. **Wei Xu:** Investigation, Writing - review & editing. **Xin Xue:** Writing - review & editing. **Conggan Yuan:** Supervision, Investigation. Priscilla **Omouendze Mouaragadja:** Supervision, Investigation. **Shan Zhao:** Supervision, Investigation. **Rodolfo Lorenzo:** Supervision, Investigation.

Conflicts of Interest

The authors declare that they have no known competing financial interests or personal relationships that could have appeared to influence the work reported in this paper.

Data Availability Statement

Some or all data, models, or codes that support the findings of this study are available from the corresponding author upon reasonable request.

References

[1] Y.X. Huang, Y.H. Ji, W.J. Yu. Development of bamboo scrimber: A literature review. Journal of Wood Science, 2019, 65(1): 1-10. https://doi.org/10.1186/s10086-019-1806-4.

[2] X.F. Sun, M.J. He, Z. Li. Novel engineered wood and bamboo composites for structural applications: State-of-art of manufacturing technology and mechanical performance evaluation. Construction and Building Materials, 2020, 249: 118751. https://doi.org/10.1016/j.conbuildmat.2020.118751.

[3] Y. Wei, M.Q. Zhou, D.J. Chen. Flexural behavior of glulam bamboo beams reinforced with near surface mounted steel bars. Materials Research Innovations, 2015, 19 (s1): 98-103. https://doi.org/10.1179/1432891715Z.0000000001377.

[4] Z. Li, M.J. He, D. Tao, M.L. Li. Experimental buckling performance of scrimber composite columns under axial compression. Composites Part B: Engineering, 2016, 86: 203-213. https://doi.org/10.1016/j.compositesb.2015.10.023.

[5] Y. Wei, S.F. Tang, X.W. Ji, K. Zhao, G.F. Li. Stress-strain behavior and model of bamboo scrimber under cyclic axial compression. Engineering Structures, 2020, 209: 110279. https://doi.org/10.1016/j.engstruct.2020.110279.

[6] H.T. Li, W. Xu, C. Chen, L.S. Yao, R. Lorenzo. Temperature influencing on the bending performance of laminated bamboo lumber. Journal of Materials in Civil Engineering ASCE, 2023, 35(5). https://doi.org/10.1061/(ASCE)MT.1943-5533.0004730.

[7] G. Chen, Y.F. Yu, X. Li, B. He. Mechanical behavior of laminated bamboo lumber for structural application: an experimental investigation. European Journal of Wood and Wood Products, 2020, 78(1): 53-63. https://doi.org/10.1007/s00107-019-01486-9.

[8] J.W. Su, H.T. Li, Z.H. Xiong, R. Lorenzo. Structural design and construction of an office building with laminated bamboo lumber. Sustainable Structures, 2021, 1(2): 000010. https://doi.org/10.54113/j.sust.2021.000010.

[9] Q.S. Zhang. Research on glued bamboo panel—I. Softening and flattening of bamboo. Journal of Nanjing Forestry University (Natural Science Edition), 1988 (4): 13-20. https://doi.org/10.3969/j.jssn.1000-2006.1988.04.002.

[10] Y.J. Li, Z.C. Lou. Progress of bamboo flatten technology research. Journal of Forestry Engineering. 2021, 6(4), 14–23. https://doi.org/10.13360/j.issn.2096-1359.202012021.

[11] T.C. Yuan, X.Z. Wang, X.R. Liu, Z.C. Lou, S.F. Mao, Y.J. Li. Bamboo flattening technology ebables efficient and value-added utilization of bamboo in the manufacture of furniture and engineered composites. Composites Part B: Engineering, 2022, 242: 110097. https://doi.org/10.1016/j.compositesb.2022.110097.

[12] D. Yang, H.T. Li, R. Lorenzo, C.G. Yuan, C.K. Hong, Y. Chen. Basic mechanical properties of laminated flattened-bamboo composite – an experimental and parametric investigation. J. Mater. Civil Eng, 2023, 35(8). https://doi.org/10.1061/JMCEE7/MTENG-15549.

[13] Y. Chen, H.T. Li, D. Yang, R. Lorenzo, C.G. Yuan. Experimental evaluation of the dowel-bearing strength of laminated flattened-bamboo lumber perpendicular to grain. Construction and Building Materials, 2022, 350: 128791. https://doi.org/10.1016/j.conbuildmat.2022.128791.

[14] H. Zhang, H.T. Li, Z.H. Xiong, O. Corbi. Experimental study and analysis of the bond-anchorage properties of laminated flattened-bamboo lumber connections with glued-in steel rod. Thin-Walled Structures, 2023, 185: 110580. https://doi.org/10.1016/j.tws.2023.110580.

[15] F. Wang, Z.P. Shao. Study on the variation law of bamboo fibers' tensile properties and the organization structure on the radial direction of bamboo stem. Industrial crops and products, 2020, 152: 112521. https://doi.org/10.1016/j.indcrop.2020.112521.

[16] K.Y. Yuan. Experimental Study on Mode I Fracture Energy of Parallel Strand Bamboo. Nanjing, China: Nanjing Forestry University, 2019. https://doi.org/10.27242/d.cnki.gnjlu.2019.000273.

[17] B.L. Sheng. Experimental and Analytical Study on Intralaminar/Interlaminar Fracture of Laminated Veneer Bamboo under Mode I Loading. Nanjing, China: Nanjing Forestry University, 2021. https://doi.org/10.27242/d.cnki.gnjlu.2021.000012.

[18] G.R. Irwin, P.C. Paris. Fundamental aspects of crack growth and fracture. Engineering fundamentals and

environmental effects. Academic Press, 1971: 1-46. https://doi.org/10.1016/B978-0-12-449703-0.50006-0.
[19] T.P.S. Reynolds, B. Sharma, E. Serrano, P.J. Gustafsson, M.H. Ramage. Fracture of laminated bamboo and the influence of preservative treatments. Composites Part B: Engineering, 2019, 174: 107017. https://doi.org/10.1016/j.compositesb.2019.107017.
[20] J.B. Leblond, A. Karma, L. Ponson, A. Vasudevan. Configurational stability of a crack propagating in a material with mode-dependent fracture energy-Part I: Mixed-mode I+III. Journal of the Mechanics and Physics of Solids, 2019, 126 (5):187-203. https://doi.org/10.1016/j.jmps.2019.02.007.
[21] G. Chen, H.Y. Luo, S.J. Wu, J. Guan, J. Luo, T.S. Zhao. Flexural deformation and fracture behaviors of bamboo with gradient hierarchical fibrous structure and water content. Composites Science and Technology, 2018, 157: 126-133. https://doi.org/10.1016/j.compscitech.2018.01.034.
[22] Y.L. An, Z.M. Liu, G. Wang, W.J. Wu. Three-point bending fracture behaviors of bamboo. In Advanced Materials Research, 2011, 261: 464-468. Trans Tech Publications Ltd. https://doi.org/10.4028/www.scientific.net/AMR.261-263.464.
[23] M.L. Chen, C.P. Dai, R. Liu, C.P. Lian, J. Yuan, C.H. Fang. Influence of cell wall structure on the fracture behavior of bamboo (Phyllostachys edulis) fibers. Industrial Crops and Products, 2020, 155: 112787. https://doi.org/10.1016/j.indcrop.2020.112787.
[24] H.R. Liu, G.Y. Peng, Y. Chai, A.Y. Huang, Z.H. Jiang, X.B. Zhang. Analysis of tension and bending fracture behavior in moso bamboo (Phyllostachys pubescens) using synchrotron radiation micro-computed tomography (SRμCT). Holzforschung, 2019, 73(12): 1051-1058. https://doi.org/10.1515/hf-2018-0275.
[25] Y.Y. Liu, B.L. Sheng, D.S. Huang, A.P. Zhou. Mode-I interlaminar fracture behavior of laminated bamboo composites. Advances in Structural Engineering, 2021, 24(4): 733-741. https://doi.org/10.1177/1369433220965270.
[26] ASTM D143-14. Standard test methods for small clear specimens of timber. USA: American Society for Testing and Materials, 2014.
[27] ASTM E399. Standard Test Method for Linear-Elastic Plane-Strain Fracture Toughness of Metallic Materials. Philadelphia, Pennsylvania, USA: American Society of Testing Materials, 2020.
[28] L. Almeida-Fernandes, N. Silvestre, J.R. Correia, M.R.T. Arruda. Fracture toughness-based models for damage simulation of pultruded GFRP materials. Composites Part B: Engineering, 2020, 186: 107818. https://doi.org/10.1016/j.compositesb.2020.107818.
[29] M.E. Toygar, F.K. Maleki. The temperature and pre-crack length effects on delamination resistance of woven GFRP sandwich composites. Mechanics, 2016, 22 (5): 331-336. https://doi.org/10.5755/j01.mech.22.5.16229.